Molecular Architecture of Plant Thylakoids under Physiological and Light Stress Conditions: A Study of Lipid–Light-Harvesting Complex II Model Membranes[C][W]

Ewa Janik,[a] Joanna Bednarska,[a] Monika Zubik,[a] Michal Puzio,[a] Rafal Luchowski,[a] Wojciech Grudzinski,[a] Radoslaw Mazur,[b] Maciej Garstka,[b] Waldemar Maksymiec,[c] Andrzej Kulik,[d] Giovanni Dietler,[d] and Wieslaw I. Gruszecki[a,1]

[a] Department of Biophysics, Institute of Physics, Maria Curie-Sklodowska University, 20-031 Lublin, Poland
[b] Department of Metabolic Regulation, Institute of Biochemistry, Faculty of Biology, University of Warsaw, 02-096 Warsaw, Poland
[c] Department of Plant Physiology, Institute of Biology and Biochemistry, Maria Curie-Sklodowska University, 20-033 Lublin, Poland
[d] Laboratoire de Physique de la Matière Vivante, Institut de Physique des Systèmes Biologiques, Ecole Polytechnique Fédérale de Lausanne, CH 1015 Lausanne, Switzerland

ORCID ID: 0000-0002-8245-3913 (W.I.G.).

In this study, we analyzed multibilayer lipid-protein membranes composed of the photosynthetic light-harvesting complex II (LHCII; isolated from spinach [*Spinacia oleracea*]) and the plant lipids monogalcatosyldiacylglycerol and digalactosyldiacylglycerol. Two types of pigment-protein complexes were analyzed: those isolated from dark-adapted leaves (LHCII) and those from leaves preilluminated with high-intensity light (LHCII-HL). The LHCII-HL complexes were found to be partially phosphorylated and contained zeaxanthin. The results of the x-ray diffraction, infrared imaging microscopy, confocal laser scanning microscopy, and transmission electron microscopy revealed that lipid-LHCII membranes assemble into planar multibilayers, in contrast with the lipid-LHCII-HL membranes, which form less ordered structures. In both systems, the protein formed supramolecular structures. In the case of LHCII-HL, these structures spanned the multibilayer membranes and were perpendicular to the membrane plane, whereas in LHCII, the structures were lamellar and within the plane of the membranes. Lamellar aggregates of LHCII-HL have been shown, by fluorescence lifetime imaging microscopy, to be particularly active in excitation energy quenching. Both types of structures were stabilized by intermolecular hydrogen bonds. We conclude that the formation of *trans*-layer, rivet-like structures of LHCII is an important determinant underlying the spontaneous formation and stabilization of the thylakoid grana structures, since the lamellar aggregates are well suited to dissipate excess energy upon overexcitation.

INTRODUCTION

In higher plants, the capturing of light energy and its conversion into forms that can be directly used to drive the metabolic reactions of living organisms, via processes of photosynthesis, takes place in the thylakoid membranes of chloroplasts (Hohmann-Marriott and Blankenship, 2011). This internal membrane system is laterally differentiated into densely stacked domains (grana) and unstacked regions (stroma lamellae) (Mustárdy and Garab, 2003; Shimoni et al., 2005; Mustárdy et al., 2008; Austin and Staehelin, 2011; Kouril et al., 2011). The thylakoid membrane is a highly dynamic system capable of adapting to changing environmental conditions. The large diameter of grana discs, high stacking of thylakoids within the granum, and large vertical distances between the stacked grana are characteristics

of low light–illuminated plants (Kouřil et al., 2012). Large-scale rearrangements of the thylakoid architecture may be caused by changes in light-harvesting complex II (LHCII) molecular organization within the lipid membrane in response to various conditions.

The molecular composition and architecture of the thylakoid membranes of plant chloroplasts are unique in several ways. Although plant thylakoid membranes are typical lipid bilayers modified with the presence of functional proteins, as in the case of other biomembranes, the proportion of protein components to lipids is extremely high. This phenomenon, referred to as "molecular crowding," can be characterized by a fraction of the entire membrane surface occupied by proteins, which can approach 70% of the plant thylakoid membrane surface and up to 80% in the grana regions of the thylakoid membranes (Kirchhoff, 2008a). Interestingly, the lipid fraction of the thylakoid membranes contains mostly monogalcatosyldiacylglycerol (MGDG; 40 to 60%), which is a non-bilayer-forming lipid, and a lesser amount of another galactolipid, digalactosyldiacylglycerol (DGDG), which is a typical bilayer-forming lipid (Wada and Murata, 2010). In the case of spinach (*Spinacia oleracea*), MGDG constitutes 57% of the thylakoid membrane lipids and DGDG constitutes 27% (Douce and Joyard, 1996). The formation of the relatively large areas of the planar lipid bilayers of the thylakoid

membranes, such as in the case of the grana structures, is thought to be possible due to the relatively high fraction of *trans*-bilayer protein components, such as LHCII, which stabilize the bilayer structure (Garab et al., 2000; Simidjiev et al., 2000).

Importantly, several of the membrane-bound antenna proteins, including LHCII, the most abundant membrane protein in the biosphere (Barros and Kuhlbrandt, 2009), are subjected to phosphorylation, in response to regulatory mechanisms that depend primarily on illumination (Allen, 1992; Iwai et al., 2008; Fristedt et al., 2009; Tikkanen and Aro, 2012). Other protein components that undergo reversible phosphorylation are D1, D2, CP43, and CP29 (Bennett, 1984; Bergantino et al., 1995). The LHCII complex is phosphorylated on the N-terminal Thr by STN7 kinase (Depège et al., 2003), which causes the complex to detach from photosystem II (PSII) in grana regions and its long-range diffusion toward the stroma lamellae. The protein phosphorylation therefore results in a dynamic, lateral reorganization of the thylakoid membranes and, consequently, in the redistribution of excitation energy between the regions enriched in the reaction centers of PSI and PSII (Fristedt et al., 2009; Tikkanen and Aro, 2012). This process is referred to as the state 1–state 2 transition. Interestingly, the process of LHCII phosphorylation has been reported to be regulated at the substrate level by light, via reversible, light-induced conformational changes (Zer et al., 1999).

Another type of light-regulated modification of LHCII is based on a change in xanthophyll composition, due to violaxanthin deepoxidation (Jahns et al., 2001; Horton, 2012). Violaxanthin deepoxidation results in the accumulation of zeaxanthin, which has been proposed to result in quenching of excessive excitations. Different molecular mechanisms of excitation quenching via zeaxanthin have been proposed. Among those mechanisms are the direct, singlet-singlet energy transfer from chlorophyll (Frank et al., 2000) and the formation of zeaxanthin-chlorophyll charge transfer complexes (Ahn et al., 2008). The indirect effect of zeaxanthin on excitation quenching in LHCII has also been proposed, based on the effect in molecular organization of LHCII supramolecular structures (Ruban et al., 1997; Gruszecki et al., 2010). Current concepts regarding molecular mechanisms involved in photoprotection in the photosynthetic antenna systems have been recently overviewed (Ruban et al., 2012).

As mentioned above, the thylakoid membranes in plant chloroplasts are involved in the formation of unique three-dimensional structures characterized by the membrane stacks called grana, connected by the thylakoid membrane of the stroma region (Mustárdy and Garab, 2003; Goral et al., 2012). Precise microscopy studies have largely elucidated the architecture of thylakoid membranes. Furthermore, the molecular principles responsible for the unique three-dimensional organization of thylakoid membranes seem to be understood (Chow et al., 2005). It is generally accepted that van der Waals interaction between the adjacent membranes involved in the formation of grana stacks as well as attractive electrostatic interactions between the opposite electric charges in those membranes are the principal forces acting to merge adjacent lipid-protein membranes into the grana structures (Chow et al., 2005). Nonphosphorylated antenna complexes are mainly localized in the grana regions of the thylakoid membranes

(Tikkanen and Aro, 2012), and the process of phosphorylation is generally thought to cause these complexes to move out of the grana, toward the unstacked regions of the thylakoids of stroma (Allen, 2003). Such a diffusion can be visualized in real time by an elegant experimental approach based on fluorescence recovery after photobleaching (Goral et al., 2010).

Here, we present the results of our microscopy-based examination of model lipid-LHCII membranes. The lipoprotein membranes can spontaneously build stacks or act toward unstacking of the adjacent membranes, depending on whether the protein components are isolated from the dark-incubated leaves or from leaves preilluminated with strong light, respectively. Moreover, the results of the molecular spectroscopy measurements show that, in addition to other possible attractive interactions, the formation of intermolecular hydrogen bonds between the polar loops of the LHCII complexes localized in the adjacent membranes provides important stabilization of grana-type membrane structures.

RESULTS

Characteristics of LHCII Preparations

Examining the influence of polypeptide phosphorylation on spectroscopic and structural properties of LHCII complexes requires pure and well-defined preparations. The high purity of the LHCII preparation was confirmed by SDS-PAGE electrophoresis and immunodetection (Figure 1), which showed the presence of Light-harvesting chlorophyll a/b-binding protein 1
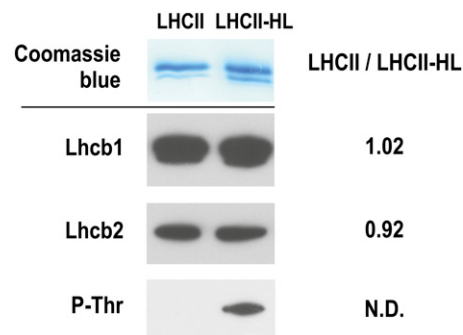

Figure 1. Characterization of Protein Components of LHCII Preparations.

Proteins were separated using SDS-PAGE (top panel) and subsequently probed against Lhcb1 and Lhcb2 proteins and phosphor-Thr residue (P-Thr; bottom panel). LHCII/LHCII-HL ratios are calculated on the basis of pixel intensity analysis. The nonphosphorylated and phosphorylated LHCII complexes were isolated from the spinach leaves dark-adapted and preilluminated for 30 min with white light of the photon flow density of 1200 μmol photons m^{-2} s^{-1}. The photon flux density, of the lamp applied, is an equivalent of 1020 μmol photons m^{-2} s^{-1} of the sunlight, in terms of a number of absorbed light quanta (see Supplemental Figure 1 online for details of this estimation). Comparative immunoblot analysis reveals 35% phosphorylation of LHCII, relative to the low-light illumination conditions (see Supplemental Figure 3 online). N.D., not determined. [See online article for color version of this figure.]

(Lhcb1) and Lhcb2 proteins. Previously, our detailed analysis of LHCII preparations obtained from dark-stored spinach leaves, by means of high performance liquid chromatography (HPLC)-electrospray ionization/mass spectrometry (Gruszecki et al., 2009a), revealed three isoforms: Lhcb1 and two Lhcb2 isoforms. The third antenna protein, Lhcb3, which was not detected by antibodies, was identified by mass spectrometry. Quantitative mass spectrometry analysis of the LHCII preparation revealed a Lhcb1/Lhcb2/Lhcb3 protein ratio of 12:6:1 (Gruszecki et al., 2009a). As shown in Figure 1, the same proportion of Lhcb1 and Lhcb2 peptides was found in both LHCII preparations (i.e., those isolated from dark-stored and light-treated spinach leaves), suggesting that the protein composition of these preparations is unchanged (see Supplemental Figure 1 online for characterization of the light treatment and Supplemental Figure 2 online for the results of gel analysis of the preparation at different stages of isolation). However, antibody was only found to interact with phospho-Thr (Figure 1) in the LHCII sample isolated from light-treated leaves, which means that this preparation contains at least a fraction of phosphorylated protein. The LHCII preparation isolated from dark-stored leaves is referred to as LHCII, while the complex isolated from leaves preilluminated with high-intensity light is referred to as LHCII-HL. A comparative immunoblot analysis revealed that a 30-min illumination with high light (1200 μmol photons m^{-2} s^{-1}) resulted in 35% phosphorylation of LHCII compared with the phosphorylation level of the LHCII complex isolated from spinach leaves illuminated for 2 h with low-intensity light (100 μmol photons m^{-2} s^{-1}; see Supplemental Figure 3 online). The chlorophyll *a* to chlorophyll *b* molar ratio in both preparations was ~1.3. The calculated molar ratios of xanthophyll per LHCII monomer (six chlorophyll *b* molecules) (see Supplemental Figure 4 online) are as follows: neoxanthin = 1.03 ± 0.17, violaxanthin = 0.65 ± 0.16, lutein 2.12 ± 0.02, zeaxanthin = not detected (LHCII), and neoxanthin = 1.0 ± 0.06, violaxanthin = 0.37 ± 0.04, lutein = 1.98 ± 0.16, and zeaxanthin = 0.16 ± 0.01 (LHCII-HL). These results reveal partial deepoxidation (~43%) of LHCII-bound violaxanthin in the LHCII-HL preparation.

Diffractometric Analysis of Lipid-Protein Samples

Lipoprotein samples were formed with both LHCII (L-LHCII) and LHCII-HL (L-LHCII-HL) and deposited to a solid support by evaporation from the aqueous suspension. The fact that the x-ray diffraction analysis was able to detect maxima in the low-angle region, corresponding to the periodicity of the samples, indicates that the deposited membranes are organized into the form of multibilayers. The presence of the protein in the lipid multibilayers increased the periodicity parameters to 6.0 nm, in the case of L-LHCII samples, and to 5.3 nm, in the case of L-LHCII-HL, compared with the sample composed of the pure lipid component (4.1 nm; Figure 2). On the other hand, the low-angle diffraction maxima of the lipid-protein samples are relatively broad, which may be associated with a presence of several slightly shifted and partially overlapped diffraction peaks corresponding to the slightly different multibilayer periodicity parameters. As can be seen, the L-LHCII sample diffractogram shows in the low-angle region not only the principal maximum
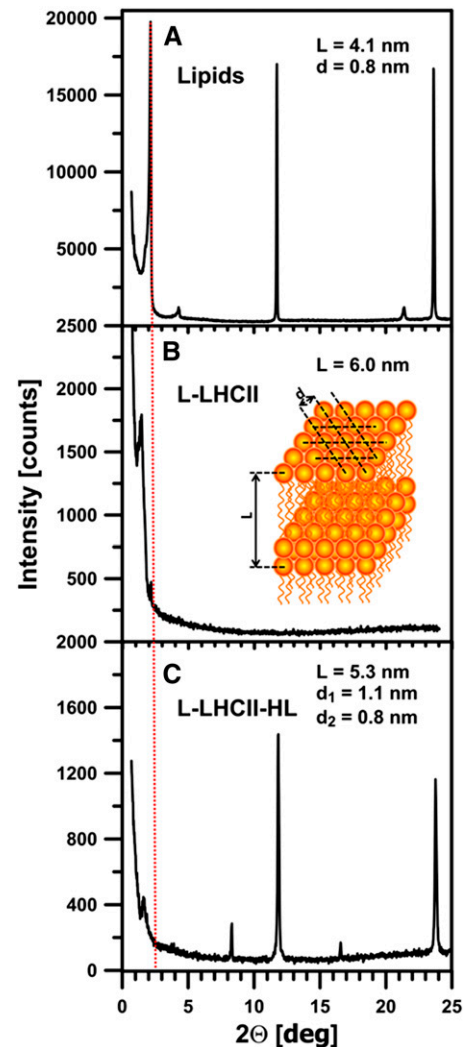
Figure 2. Diffractometric Analysis of Lipid-Protein Multibilayers.

Original diffractograms of lipid (MGDG+DGDG) multibilayers modified with LHCII complexes. Red vertical dashed line indicates the low-angle maximum corresponding to the periodicity of the multibilayer formed with pure lipids. The inset is a schematic representation of a part of the lipid multibilayer. Parameters L and d refer to the Bragg's spacing related to the low-angle and wide-angle diffraction maxima, respectively. The value of parameters L and d were determined on the basis of a position of diffractometric maxima according to Bragg's law. Note the two different d spacing parameters determined in the case of the L-LHCII-HL multibilayers.

(A) Multibilayers composed of the mixture of MGDG and DGDG in a molar ratio of 2:1 (Lipids).
(B) Lipid multibilayers modified with LHCII complexes isolated from dark-incubated leaves (L-LHCII).
(C) Lipid multibilayers modified with LHCII complexes isolated from leaves preilluminated with high-intensity light (L-LHCII-HL).
[See online article for color version of this figure.]

related to the periodicity parameter L = 6.0 nm but additionally the relatively small maximum at the $2\Theta = 2.18°$, corresponding to the pure lipid multibilayer (L = 4.1 nm). Such an additional maximum is not observed in the case of the L-LHCII-HL samples. This observation is consistent with the conclusion that both phases appear in the L-LHCII multibilayer samples: the LHCII-modified phase and the protein-free lipid phase. Interestingly, the wide-angle diffraction maxima, corresponding to the lipid headgroup packing (spacing parameter d = 0.8 nm) (Gruszecki and Sielewiesiuk, 1991), are not observed in the L-LHCII samples, in contrast with the multibilayers formed both with the pure lipids and L-LHCII-HL. In the case of the L-LHCII-HL sample, two sets of shifted diffractometric maxima have been observed, corresponding to different parameters d: one corresponding to the pure lipid phase (d = 0.8 nm) and another one, greater (d = 1.1 nm; Figure 2), corresponding to the lipid phase modified by the presence of the protein component. The different organization of the lipid phase in the L-LHCII-HL samples reflects the effect of the protein component on molecular organization of multibilayers. The lack of low-angle diffraction maxima in L-LHCII is an indication that, to a large extent, the samples remain in the form of the planar multibilayers, oriented horizontally within the plane of the solid support. The larger periodicity observed for such structures can be interpreted in terms of an ordering effect of the protein with respect to the hydrophobic lipid bilayer core and/or in terms of location of the polar fragments of LHCII in the interbilayer space of the multilayer. The fact that the protein effect on the multilayer

periodicity is more pronounced in the case of L-LHCII than in the case of L-LHCII-HL can be interpreted as an indication that the polar fragments of the protein molecules, present in the adjacent bilayers, interact with each other, thus influencing, in a concerted way, the multibilayer organization. The smaller effect observed in the case of L-LHCII-HL indicates that such an interaction between the complexes in the adjacent layers does not take place. This is most probably due to the electrostatic repulsion of the phosphate groups present in the LHCII-HL preparation. The model of the organization of the L-LHCII and L-LHCII-HL multibilayers, corresponding to the results of the diffractometric analysis, is presented in Figure 3.

Infrared Analysis of the Lipid-Protein Multibilayers

Infrared (IR) absorption imaging of L-LHCII and L-LHCII-HL multibilayers was performed to test the protein arrangement proposed in the model presented in Figure 3. The rationale of such an experiment was based on the expectation that the putative formation of integrated *trans*-layer structures, by vertically aligned LHCII molecules (trimers), should result in enhanced IR absorption in the spectral region corresponding selectively to proteins (e.g., amide I region; see below). A more homogenous distribution of the protein component in the L-LHCII-HL samples, along the direction perpendicular to the multibilayer, should result in a lack of such distinctive IR absorption regions of the protein. Figure 4 presents the results of the IR imaging of the L-LHCII and L-LHCII-HL multibilayers,
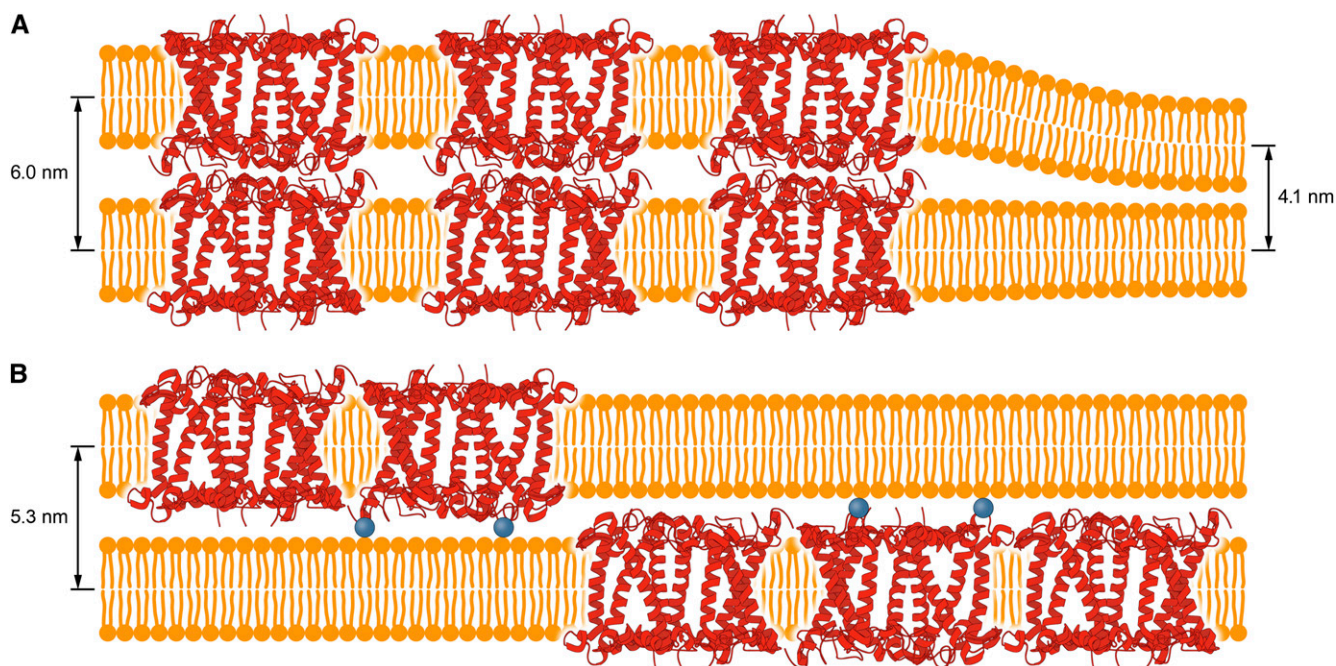

Figure 3. Model of Molecular Organization of the Lipid-Protein Membranes.

The model refers to the membranes formed with LHCII isolated from dark-adapted leaves **(A)** and leaves preilluminated with high-intensity light **(B)**. Phosphorylation of Thr at the N terminus of LHCII peptide is depicted by blue balls. The diffractometrically determined multibilayer periodicity parameters are shown. For clarity, only the protein components of LHCII is shown.
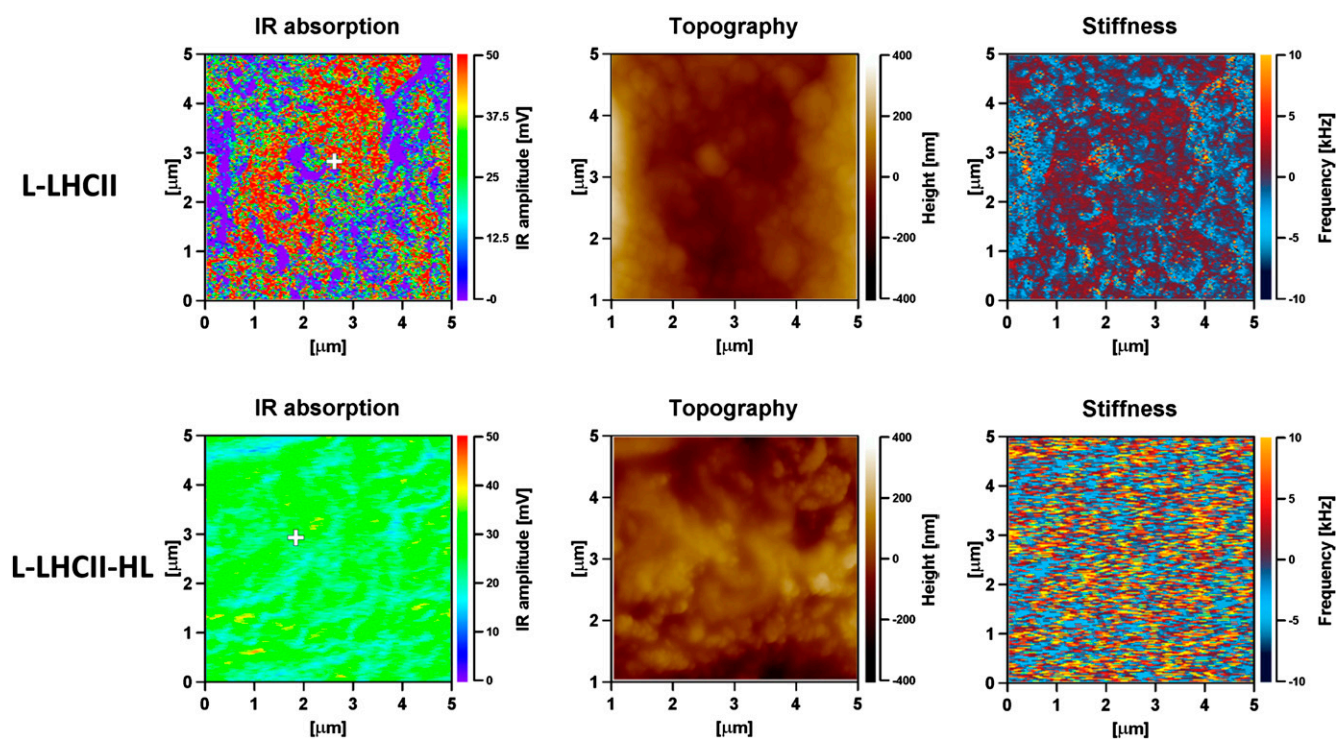[See online article for color version of this figure.]

Figure 4. IR Absorption, Topography of the Surface, and Mechanical Stiffness Images, Recorded Simultaneously from the 5 × 5-μm area of the Lipid-Protein Multibilayer Deposited at the ZnSe Surface, Formed with LHCII Isolated from Dark-Incubated Leaves and Leaves Preilluminated with High-Intensity Light.

The samples formed with LHCII are referred to as L-LHCII and formed with LHCII-HL are referred to as L-LHCII-HL. The maximum thickness of the sample was 1.5 μm. The IR absorption was scanned at 1650 cm^{-1}. The white crosses indicate the places in the samples at which the IR absorption spectra were recorded (displayed in Figure 5). Scan resolution X, 512 points; Y, 256 points; and scan rate 0.4 Hz, eight coaverages.

using the atomic force microscopy (AFM)–detected IR absorption technique (IR-AFM) (Policar et al., 2011). The AFM-determined height of the layers examined was ~1.5 μm, which means that the samples consisted maximally of 250 bilayers. As can be seen, the L-LHCII multilayer contains regions characterized by a relatively high concentration of the protein (marked red), distributed heterogeneously within the plane of the sample. These are in turn accompanied by regions with relatively high concentration of lipids and relatively low concentration of LHCII (marked violet). The L-LHCII-HL multilayers are characterized by a more homogenous protein distribution and by the lack of regions of relatively high protein concentration along axes perpendicular to the plane of the sample. The presence of LHCII and lipids is represented by the pronounced band in the amide I spectral region (1600 to 1700 cm^{-1}) and ester carbonyl stretching vibrations with the maximum at 1727 cm^{-1}, respectively (Gruszecki et al., 2006, 2009b). This can be seen from the IR absorption spectra recorded from the multibilayer samples (Figure 5). Further analysis of the samples revealed that the protein-containing regions of the samples are characterized by the higher mechanical stiffness (Figure 4). The fact that IR imaging of the lipid-protein multibilayers shows the regions of a relatively high LHCII concentration exclusively in the case of the L-LHCII samples and more homogeneous protein distribution in

the case of the L-LHCII-HL samples, provides strong support to the concept of formation of the integrated, *trans*-layer structures by nonphosphorylated LHCII, which does not contain zeaxanthin. The results of the control IR-AFM analysis of the multibilayer formed with pure lipid components are presented in Supplemental Figure 5 online.

Figure 6 shows the macroscopic IR absorption spectra (Fourier transform infrared absorption spectroscopy [FTIR]) of the L-LHCII and L-LHCII-HL samples in the amide I region. Despite similarity of the spectra, certain small but significant differences can be noticed. The differences are distinctively pronounced in the difference spectrum presented in Figure 6B. As can be seen, L-LHCII-HL is characterized by higher intensities in the spectral band with the maximum in the region of 1620 cm^{-1}. This region can be assigned to the lamellar aggregated structures of LHCII (Gruszecki et al., 2009b). On the other hand, the L-LHCII samples are characterized by higher intensities in the spectral band with the maximum at 1688 cm^{-1}. This spectral region can be formally attributed to antiparallel β-sheet structures (Tamm and Tatulian, 1997), and it represents, most probably, the β-like structures stabilized by the hydrogen bonds between the polar loops of the LHCII complexes involved in the formation of the *trans*-layer, integrated supramolecular structures.
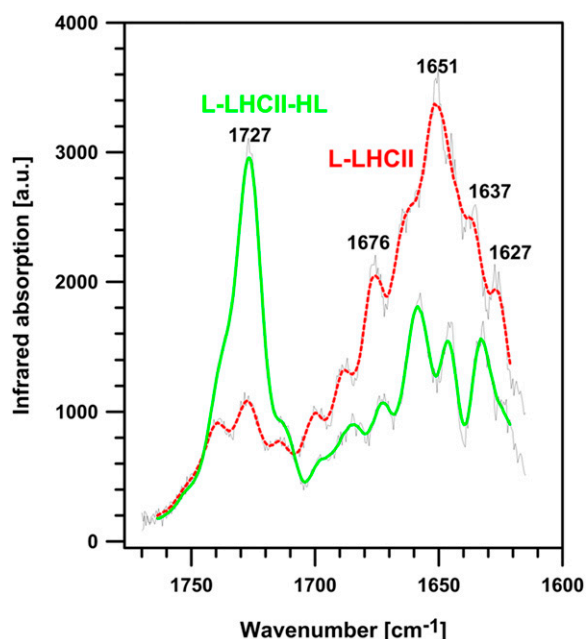
Figure 5. IR Absorption Spectra Recorded from the Lipid-Protein Multibilayer Samples L-LHCII and L-LHCII-HL.

The spectral region corresponds to the white crosses in Figure 4: The spectrum drawn with red dashed line was recorded from the L-LHCII sample, and the spectrum drawn with green solid line was recorded from the L-LHCII-HL sample (marked). The spectra were recorded in the amide I region of the protein (1600 to 1700 cm^{-1}) and in the ester carbonyl stretching region of the lipid components (1700 to 1750 cm^{-1}). The reference spectrum from the pure buffer evaporated at the surface of the ZnSe crystal was recorded in the same spectral range and under the same conditions. The original spectra are presented with gray lines, superimposed on the processed spectra obtained by smoothing by the Savitzky-Golay procedure (second order polynomial, 15 points). The spectra were recorded with a resolution of 0.5 cm^{-1}, sample rate 12.5 MHz, and 256 coaverages. a.u., arbitrary units.
[See online article for color version of this figure.]

Fluorescence Analysis of Lipid-Protein Samples

Figure 7 presents the chlorophyll *a* fluorescence emission spectra, recorded at 77K from the L-LHCII and L-LHCII-HL samples. As can be seen, both spectra show enhanced intensity in the region of 700 nm, typical of aggregated LHCII (Ruban et al., 1995; Zubik et al., 2013). The fact that the 700-nm band is particularly intensive in the L-LHCII-HL samples corroborates the observation that this band corresponds to the aggregated structures of LHCII formed in the plane of the lipid-protein bilayer (Zubik et al., 2013). As can be expected, such structures give rise to the shortened chlorophyll *a* fluorescence lifetimes. This can be seen from the fluorescence decay distribution analysis presented beneath the fluorescence lifetime imaging microscopy (FLIM) scans in Figure 8. The FLIM analysis of both the L-LHCII and L-LHCII-HL samples reveals a relatively homogeneous distribution of the spectral forms characterized by the fluorescence emission lifetimes (Figure 8, top panel). The

fluorescence lifetime distributions are relatively narrow. As can be seen, the maximum in distributions appears at a much shorter lifetime (~0.7 ns) in the case of L-LHCII-HL compared with the lifetime distribution corresponding to the L-LHCII particle (~1.3 ns). The intensity-weighted average fluorescence lifetime values based on the three-component analysis (Figure 8, bottom panel) are 0.78 and 1.06 ns in the case of the L-LHCII-HL and L-LHCII samples, respectively. The lifetimes are distinctly different despite the fact that the LHCII-HL preparation contains a large fraction of nonphosphorylated protein and that only 43% of the violaxanthin pool has been replaced by zeaxanthin. The chlorophyll *a* fluorescence lifetimes in both types of samples are distinctly shorter than in the case of trimeric LHCII in the detergent solution (<τ> = 3.5 ns; van Oort et al., 2007) but in the order of magnitude of the protein in the model lipid membrane environment (<τ> = 1.01 ± 0.02 ns; Zubik et al., 2013) and in natural thylakoid membranes of *Arabidopsis thaliana* (<τ> = 0.9 ± 0.1 ns, in the non-photochemical quenching (NPQ) state; Belgio et al., 2012).
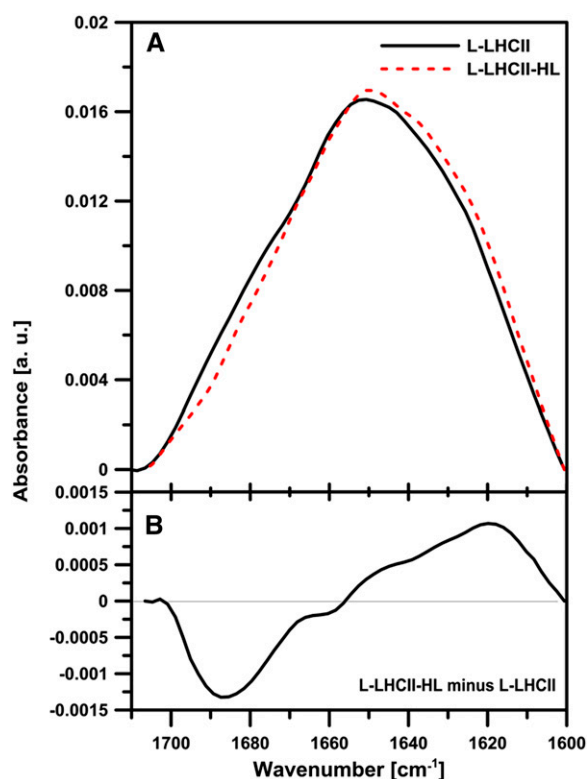

Figure 6. IR Absorption Analysis of L-LHCII and L-LHCII-HL Samples.

(A) Infrared absorption spectra (FTIR) in the amide I region of the lipid-protein multibilayers L-LHCII (solid line) and L-LHCII-HL (dashed line). The spectra were normalized to get the same area beneath each spectrum.
(B) Different spectrum calculated on the basis of the spectra presented in the top panel. a.u., arbitrary units.
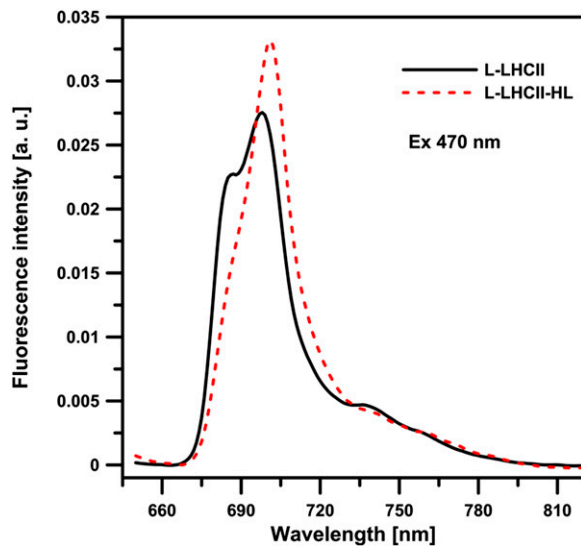[See online article for color version of this figure.]

Figure 7. 77K Chlorophyll *a* Fluorescence Emission Spectra Recorded from the Lipid-Protein Samples L-LHCII and L-LHCII-HL.

The spectrum corresponding to the L-LHCII sample is plotted with solid line, and the spectrum corresponding to the L-LHCII-HL sample is plotted with dashed line. Excitation wavelength was at 470 nm. The spectra were normalized to get the same area beneath each spectrum. a.u., arbitrary units.

[See online article for color version of this figure.]

Confocal Laser Scanning Microscopy of Lipid-Protein Samples

Visualization of chlorophyll *a* fluorescence by confocal laser scanning microscopy (CLSM) enabled observation of the natural lipid membranes containing the chlorophyll-protein complexes (e.g., inside intact chloroplasts or leaves) without any fixation procedure and in situ (Mehta et al., 1999; Garstka et al., 2005, 2007; Hasegawa et al., 2010; Rumak et al., 2010, 2012). Red fluorescence was attributed mainly to chlorophyll *a* species emitted at around 680 nm, because at room temperature the long-wavelength emission, above 700 nm, was rather weak (Mehta et al., 1999; Hasegawa et al., 2010). In our case, the CLSM images revealed the chlorophyll *a* fluorescence from LHCII incorporated into model lipid bilayers (Figure 9). Furthermore, the three-dimensional distribution of fluorescence depicted the real spatial interaction between membranes.

In the LHCII-containing membranes, most of the red fluorescence intensities are evenly distributed in the irregular cloud of chlorophyll *a* fluorescence. In the case of the L-LHCII samples, certain, not clearly separated structures, characterized by relatively higher fluorescence intensity, can be observed, spanning the entire lamella-like sample (Figure 9A; see Supplemental Movie 1 and Supplemental Movie Legend 1 online). In the case of L-LHCII-HL, the sample is clearly not organized into a lamellar shape (Figure 9B). In this case, the condensation of chlorophyll *a* fluorescence into brightly red fluorescent discs is observed, only with slight fluorescence dispersion. Moreover, the irregularly distributed red areas are clearly separated by dark space

(Figure 9B). Because the chlorophyll *a* fluorescence is strictly attributed to light-harvesting complexes, the CLSM images revealed distribution of LHCII or LHCII-HL complexes in lateral and vertical planes of the lipid-protein multibilayers.

Large numbers of fluorescence images were taken in different focal depths (Garstka et al., 2005, 2007; Rumak et al., 2010, 2012). This allowed the creation of computer-generated three-dimensional structures in which the spatial layout of chlorophyll *a* fluorescence intensity was shown. The surface of chlorophyll *a* fluorescence areas is shown from the front and side (Figures 9C to 9F). The three-dimensional models of the multibilayer samples highlighted the tendency observed directly by CLSM (see Supplemental Movies 1 and 2 and Supplemental Movie Legends 1 and 2 online).

A spatial model for L-LHCII shows a wrinkled and irregular flat disk of stacks, with a diameter of ~7 μm and <0.5 μm thick (Figures 9C and 9E). This indicates that these bilayers formed the continuous surface, where neighboring membranes fit tightly on a long distance. Since the stack of two adjacent thylakoid membranes, mostly containing LHCII as a protein component, is ~17 nm high (Kirchhoff et al., 2008a; Rumak et al., 2010), the stacks of L-LHCII should be composed from ~20 membrane pairs (Figure 9E). A similar conclusion can be reached based on the diffractometrically determined periodicity parameter of the multibilayer, taking into account the relatively broad diffraction maxima observed in the case of the L-LHCII samples (Figure 2). Quite a different structure was created by the L-LHCII-HL stacks (Figures 9D and 9F). The layout of chlorophyll *a* fluorescence forms many clearly distinguished egg-shaped areas with a diameter of ~0.5 μm. These merge only at the edge, but some ovals are not connected with the others (Figure 9F). It might be suggested that the adjacent membranes in the L-LHCII-HL are weakly connected in a stack due to electrostatic and hydration repulsion between membranes (Rumak et al., 2010). The general view of the model revealed that relatively small L-LHCII-HL stacks are evenly arranged in all axes of three-dimensional space, forming a wide three-dimensional cluster (Figure 9F). The formation of the small three-dimensional structures, characterized by a relatively intensive chlorophyll *a* fluorescence in the L-LHCII-HL samples, can be interpreted in terms of the formation of lamellar LHCII-HL aggregated structures. The size of such structures (~250 nm) is in the optical microscopy limit and does not allow us to determine the precise number of LHCII-HL trimers involved in the formation of the supramolecular structures.

Certain size and shape parameters may be determined in three-dimensional fluorescence models. The ratio of surface area to total volume (A/V) was calculated for both models of the samples, L-LHCII and L-LHCII-HL. Eight independent models for each experimental variant were analyzed. This parameter was estimated to be 3.84 ± 0.35 for L-LHCII and 4.83 ± 0.48 for L-LHCII-HL (P < 0.0003). Because chlorophyll *a* fluorescence is related to the amount of light-harvesting complexes as well as to the length and height of lipid-protein stacks, the A/V ratio indicated the surface irregularity and unfolding degree of stacks (Rumak et al., 2012). Thus, these calculations confirm the observations (Figure 9) that in L-LHCII stacks the adjacent membranes are tightly connected, while in L-LHCII-HL, the membranes
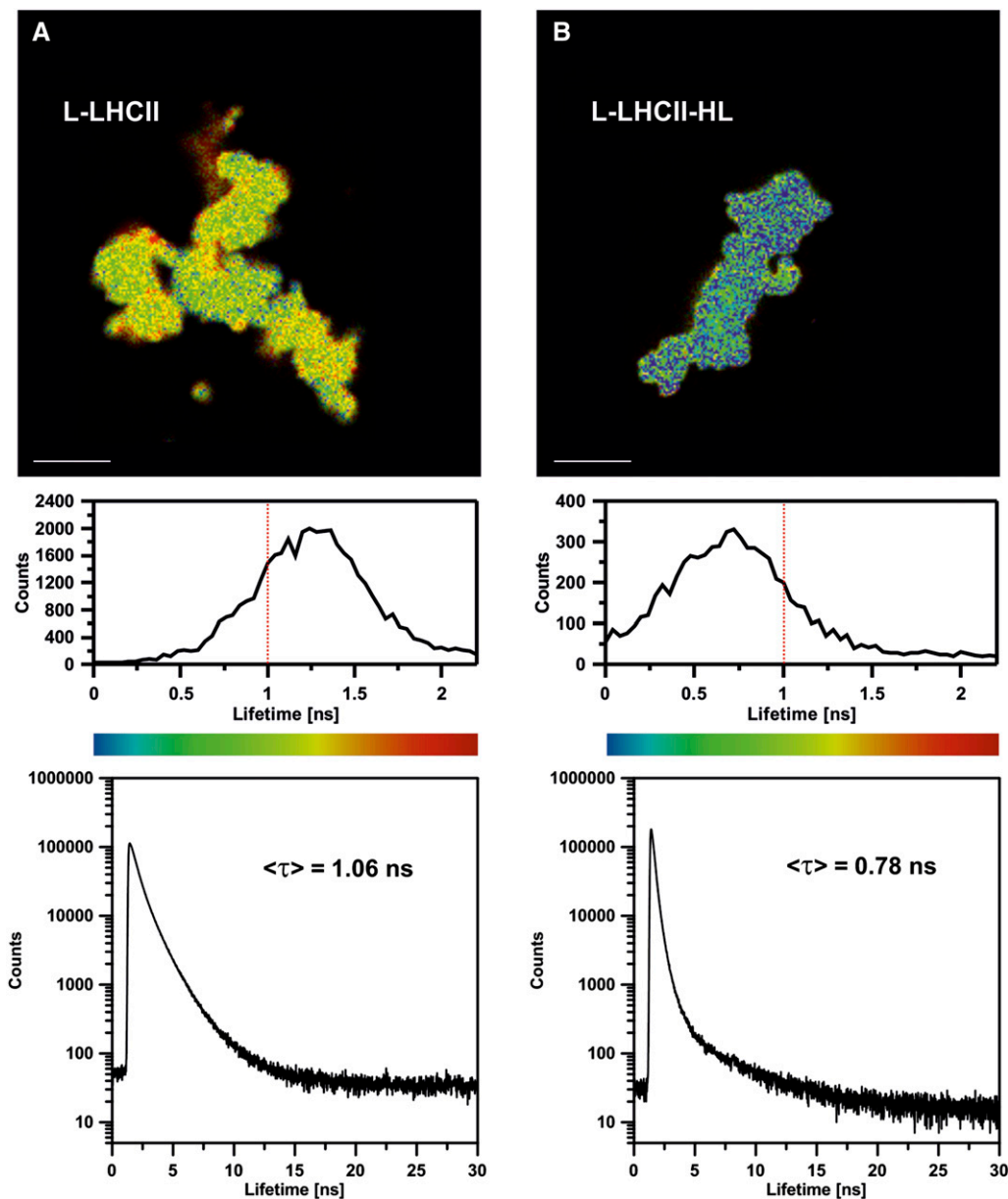
Figure 8. FLIM Images of the 60 × 60-μm Areas of the Glass Slides Covered with Poly-ʟ-Lys, on Which L-LHCII and L-LHCII-HL Particles Were Deposited from the Aqueous Suspensions of the Samples Diluted to Micromolar Concentration of LHCII.

Fluorescence lifetime distribution (middle panel) and fluorescence decay traces (bottom panel) were presented below each image. The intensity-weighted average lifetimes (<τ>) of each scanned sample are displayed, based on the three component deconvolution: 0.49, 1.19, and 3.78 ns (χ^2 = 1.003) in the case of L-LHCII and 0.24, 0.59, and 3.78 ns (χ^2 = 1.044) in the case of L-LHCII-HL. Lifetime threshold corresponding to 1 ns is marked in histograms by red dashed line. Bars = 10 μm.

are partially separated and the protein clusters are rather formed in the plane of each membrane.

For a better view of the three-dimensional structure of preparations, animated models are included in Supplemental Movies 1 (L-LHCII) and 2 (L-LHCII-HL) and Supplemental Movie Legends 1 and 2 online.

The CLSM results showing that the L-LHCII samples can organize into multilayer structures, in contrast with the L-LHCII-HL

samples, were confirmed by an analysis of transmission electron microscopy images (Figure 10).

DISCUSSION

The samples examined in this study were formed by a self-organization of the mixture of chloroplast lipids (MGDG with
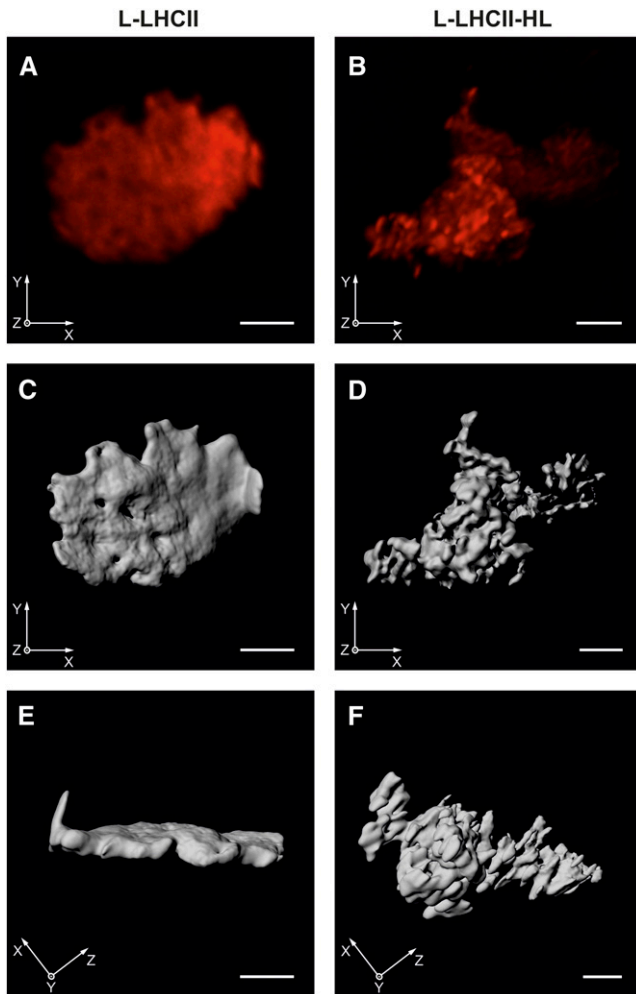
L-LHCII   L-LHCII-HL

Figure 9. Chlorophyll *a* Fluorescence of Lipid-LHCII Samples Revealed by CLSM and Subsequent 3D Reconstruction.

The L-LHCII **(A)** or L-LHCII-HL **(B)** samples were incubated in buffered medium containing 10 mM KCl. Each red image presents the sum projection of deconvolved stack of CLSM. Gray images represent three-dimensional models of the L-LHCII (**[C]** and **[E]**) or L-LHCII-HL (**[D]** and **[F]**) created after deconvolution. Face (**[C]** and **[D]**) and rotated (**[E]** and **[F]**) view of three-dimensional sample models is shown. Bars = 2 μm. [See online article for color version of this figure.]

DGDG) and LHCII complexes isolated from spinach chloroplasts. Formation of the lipid-protein systems was achieved by slowly removing detergent from the aqueous suspension. The procedure yielded relatively small, LHCII-containing membrane fragments (17 to 83 nm; see Supplemental Figure 6 online), which can assemble into lipid-protein multibilayers when deposited on a solid support. Such structures are two-component, mixed lipid-protein systems. This conclusion is based on the analysis of the x-ray diffractograms (Figure 2). The positions of the diffractometric maxima show the appearance of the new lipid-protein multibilayer phases, created upon incorporation of LHCII, at the expense of the intensity of the maxima characteristic

for the pure lipid phase. Moreover, the fluorescence microscopy analysis of the emission originating from the LHCII-bound chlorophyll molecules and from the fluorescence label molecules embedded in the lipid phase shows colocalization over the entire lipid-LHCII sample volume (see Supplemental Figure 7 online).

Two types of antenna complexes were studied, those isolated from leaves that were dark adapted (LHCII) and preilluminated with high intensity light (LHCII-HL). The immunostaining analysis showed that 35% of the LHCII pool was phosphorylated in such a sample after the strong light treatment compared with the LHCII phosphorylation level evoked by illumination with low light intensity (see Supplemental Figure 3 online). This observation corroborates the finding that the maximum phosphorylation of LHCII in spinach can be achieved during illumination with relatively low light intensity ($\sim$100 μmol photons m^{-2} s^{-1}) and decreases following an increase in light intensity (Rintamäki et al., 1997). The pigment composition analysis shows that 43% of the violaxanthin present in the LHCII preparation is replaced by zeaxanthin in the LHCII-HL samples. The results of our spectroscopic measurements show that both the LHCII preparations, isolated from dark-adapted and preilluminated leaves, do not differ significantly. This can be seen from the comparison of the chlorophyll *a* fluorescence lifetime analysis and emission spectra recorded both from LHCII and LHCII-HL in a trimeric form (see Supplemental Figure 8 online). On the other hand, the LHCII organization in a lipid-protein system is distinctly different and gives rise to pronounced differences in protein organization, manifested by chlorophyll *a* fluorescence lifetimes, 77K fluorescence emission spectra, and FTIR spectra.

Diffractometric analysis of the samples deposited on a solid support by evaporation from aqueous suspensions has shown that both samples, L-LHCII and L-LHCII-HL, are at least partially organized into multibilayers. The periodicity of the multibilayers formed with pure lipid mixture, determined to be 4.1 nm, was distinctly lower than that observed in the case of the system composed of lipids and LHCII-HL (5.3 nm) or composed of lipids and LHCII (6.0 nm). Interestingly, in the case of L-LHCII, the diffractometric technique has shown additionally the formation of oriented lamellar multibilayer structures. Moreover, the ability of the L-LHCII system to form such structures has been
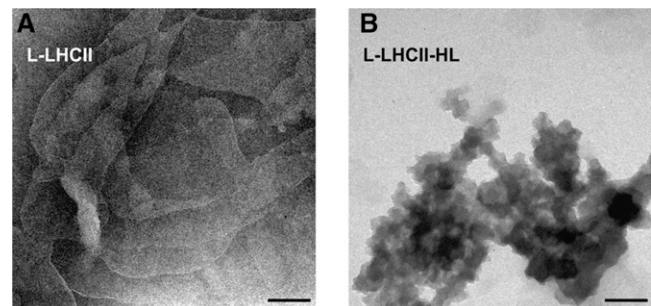

Figure 10. Transmission Electron Microscopy Images of the L-LHCII and L-LHCII-HL Samples.

L-LHCII **(A)** and L-LHCII-HL **(B)** samples. Bars = 200 nm.

concluded based on the results of CLSM and electron microscopy. All the measurements, outlined above, have been integrated into the schematic model of organization of the lipid-protein multibilayers binding LHCII isolated from dark-adapted and preilluminated leaves (Figure 3). As depicted in the model, in the L-LHCII lamellar samples, the protein molecules are organized within the supramolecular structures, which are aligned vertically with respect to the plane of the multibilayer. The formation of such *trans*-layer structures has been exclusively observed in the case of the L-LHCII samples, but not in the case of the L-LHCII-HL samples, most probably owing to the electrostatic repulsion of the negatively charged phosphate groups. Such an observation has strong support from the microscopy imaging based on IR absorption (Figure 4). The IR-AFM technique showed, in the case of the L-LHCII layers, the distinct areas characterized by a relatively high protein concentration, sharply separated from the areas characterized by domination of the lipid component. This observation is consistent with the accumulation of a large number of LHCII complexes along axes perpendicular to the plane of the scanned sample. Such a conclusion can be drawn due to the fact that the IR-AFM technique is sensitive to a concentration of probed molecules, located beneath the AFM tip (Policar et al., 2011; Lahiri et al., 2013). A comparative analysis of the FTIR spectra recorded from the L-LHCII and L-LHCII-HL multibilayers shows that the *trans*-layer, supramolecular structures formed by the nonphosphorylated complexes, which do not contain zeaxanthin, are stabilized by intermolecular hydrogen bonds, which give rise to the antiparallel β-like structures, corresponding to the IR absorption band centered in the region of 1688 cm^{-1} (Figure 6B). Most probably, the protein loops localized in the interbilayer region are responsible for the formation of such bonds. On the other hand, the protein components in the L-LHCII-HL samples were found to be involved in the formation of another type of supramolecular structure, stabilized by intermolecular hydrogen bonds, which give rise to the IR absorption band centered in the region of 1620 cm^{-1} (Figure 6B). Such aggregates of LHCII have been referred to as lamellar supramolecular structures formed in the plane of monomolecular layers (Gruszecki et al., 2009b). Interestingly, formation of such aggregated structures of LHCII has been reported to be facilitated by the presence of zeaxanthin (Ruban et al., 1997; Gruszecki et al., 2006, 2010). Enhanced formation of the lamellar aggregated structures in the L-LHCII-HL samples is corroborated by the presence and relatively high intensity of the band at ~700 nm, in the 77K fluorescence emission spectra of chlorophyll *a* (Figure 7), and by shortened chlorophyll *a* fluorescence lifetimes (Figure 8). The absence of such a high number of lamellar aggregates of LHCII, in the samples composed of nonphosphorylated protein, can be explained in terms of involvement of the complex molecules in formation of the *trans*-layer structures, which naturally limits diffusional freedom of the protein complexes within the individual lipid bilayers and therefore limits formation of the diffusion-controlled protein assemblies. The absence of zeaxanthin in the LHCII samples has to be also considered as a potential determinant of molecular organization of the protein, in light of the finding that this xanthophyll promotes formation of lamellar molecular structures (Ruban et al., 1997; Gruszecki

et al., 2006, 2010). An important consequence of assembling of LHCII complexes, into the *trans*-layer structures, stabilized by intermolecular hydrogen bonds, and, therefore, relatively stable, seems to be the formation of the rivet-like structures, linking adjacent bilayers to the membrane stacks. The formation of such stable lamellar membrane stacks has been confirmed by the results of the microscopy analyses, which include CLSM (Figure 9) and transmission electron microscopy (Figure 10). Microscopy techniques, and in particular CLSM, show close similarities in the organization of natural chloroplast membranes and the model systems studied in this work (Rumak et al., 2010, 2012). In particular, the process of grana stack formation by the thylakoid membranes appeared to have its analog in the model system composed of the mixture of chloroplast lipids (MGDG with DGDG, 2:1) and nonphosphorylated and zeaxanthin-lacking LHCII isolated from dark-adapted leaves. It has to be emphasized that the protein-lipid molecular fraction ratio (1:20) has been selected to mimic exceptionally high molecular crowding in the natural thylakoid membranes and to reach 70 to 80% occupation of the membrane surface by the protein component (Kirchhoff, 2008a, 2008b; Kirchhoff et al., 2008a, 2008b) (see Supplemental Methods 1 online for details of the calculation of the protein area fraction). The formation of grana structures in chloroplasts of higher plants can be understood in terms of the interplay of physicochemical forces of attraction and repulsion (Chow et al., 2005). The van der Waals interaction and the coulombic interactions of opposite electric charges located on adjacent membranes are considered to be among the principal attractive forces responsible for the formation of grana in chloroplasts (Chow et al., 2005). In this work, we show that the grana-like structures can be formed by the self-organization of lipid-protein membranes comprising the major plant antenna complex LHCII and that such structures are stabilized by a hydrogen bond network between the polar loops of the protein. Such a hydrogen bond network results in the formation of the column-shaped LHCII structures, spanning vertically the grana-like discs and therefore providing stabilization of a multibilayer structure in a skeleton-type fashion. Interestingly, such structures cannot be formed when LHCII isolated from leaves preilluminated with high-intensity light is used as a protein component of the model membranes, even when violaxanthin deepoxidation is only partial and a relatively small fraction of the complexes is phosphorylated. This suggests that the state 1–state 2 transition, which relies on antenna protein phosphorylation and dynamically regulates excitation energy distribution within the thylakoid membrane system and optimal mobility of the PSII-LHCII protein complexes along the thylakoid membrane (Tikkanen and Aro, 2012) can also be involved in the dynamic regulation of the three-dimensional organization of the thylakoid membranes. In this context, it is worth emphasizing that increased membrane folding, caused by the loss of light-induced protein phosphorylation, has been observed in *Arabidopsis* (Fristedt et al., 2009). Our observation that nonphosphorylated LHCII complexes, which do not contain zeaxanthin, can be involved in the formation of the hydrogen bond network between adjacent lipid-protein membranes fits the concept of dynamic reorganization of the chloroplast membrane architecture, which involves fusion and fission events that occur between the

nonappressed and appressed thylakoid membranes (Chuartzman et al., 2008). On the other hand, the fact that the zeaxanthin-containing and partially phosphorylated LHCII pool has a much higher affinity to form lamellar aggregated structures in the lipid phase, as demonstrated in this work, seems also to have a pronounced consequence from the physiological standpoint. Since antenna protein phosphorylation results in the energetic uncoupling from the PSII reaction center, the fraction of LHCII that actively absorbs light energy and at the same time is not energetically coupled to any of the reaction centers, cannot transfer excitation energy outside, and therefore is subjected to severe risk of overexcitation and oxidative damage. As shown above, complexes from such a pool, readily form lamellar supramolecular structures, which are characterized by efficient singlet excitation quenching (Zubik et al., 2013). Owing to this fact, the process of molecular assembly of zeaxanthin-containing and partially phosphorylated LHCII seems to have particular importance in photoprotection of this antenna complex. Interestingly, FLIM-based imaging of live green algae cells has revealed that LHCII phosphorylation is followed by the formation of aggregated structures of this pigment-protein complex characterized by enhanced excitation quenching (Iwai et al., 2010).

An important role of light-induced LHCII reorganization in photoprotection against light-induced damage has emerged from several studies, both in vivo and in vitro (Barzda et al., 1996; Dobrikova et al., 2003; Cseh et al., 2005; Holm et al., 2005; Gruszecki et al., 2009b; Johnson et al., 2011). Most of these data suggest that the primary site of light-induced reorganizations is on the outer loop segments of LHCII, affecting the phosphorylation (Zer et al., 1999), the cation binding sites (Cseh et al., 2000; Garab and Mustardy, 2000), and the ability of stacking and lateral reorganizations (Dobrikova et al., 2003; Gruszecki et al., 2009b). Despite the differences in xanthophyll composition and phosphorylation status of the LHCII and LHCII-HL samples, both the fluorescence emission spectra and the fluorescence lifetimes are almost identical (see Supplemental Figure 8A online). By contrast, the spectroscopy analyses show pronounced differences between the lipid-protein samples prepared with those two types of complexes. This fact corroborates a central role of organization of the protein in the management of excitations in the photosynthetic apparatus.

Interestingly, relatively low light intensity ($\sim$100 µmol photons $m^{-1}\ s^{-1}$), corresponding to half the light intensity used to irradiate spinach leaves during growth, was shown to induce a maximum phosphorylation of the LHCII pool (Rintamäki et al., 1997). The physiological importance of such a mechanism could be associated with the excitation energy redistribution between the grana and stroma regions of the thylakoid membranes, which are enriched in the PSI and PSII reaction centers (Tikkanen et al., 2011), molecular remodeling of PSII (Iwai et al., 2008), and possibly also in disassembly of supramolecular structures of LHCII, which can be present in the photosynthetic apparatus and are known to quench chlorophyll singlet excitations efficiently. Such disassembly can be simply driven by lateral electrostatic repulsion between the negatively charged phosphorylated protein complexes (Allen, 1992). Elimination of the excitation quenching in LHCII, via disassembly of supramolecular

structures, can be recognized as a vital process under low-light conditions associated with a relatively low excitation density. On the other hand, illumination with strong light can be associated with photoinhibition and photodamage. As has been reported (Rintamäki et al., 1997), the phosphorylation level of the PSII core complexes remains high under strong light conditions, whereas the LHCII pool becomes dephosphorylated to a relatively low level.

The spectroscopy results presented in this work show that such a low phosphorylation level of the LHCII pool, combined with violaxanthin deepoxidation, prevent the formation of the transmembrane structures and promote the formation of the lateral supramolecular structures within each membrane, which are characterized by a relatively high yield of excitation quenching.

The latter mechanism can be considered as an important element of the photoprotection strategy in the photosynthetic apparatus of plants under overexcitation conditions.

Concluding Remarks

We studied the model lipid-protein membranes consisting of chloroplast lipids and the antenna complex LHCII. Membranes containing LHCII isolated from dark-adapted leaves assembled into lamellar stacks in which the protein molecules form the *trans*-layer supramolecular structures. The rivet-like structures are stabilized by intermolecular hydrogen bonds and can serve as a scaffold for the lipid-protein membrane stacks. The formation of such lipid-protein structures has not been observed in partially phosphorylated LHCII isolated from leaves preilluminated with high-intensity light. In such complexes, a fraction of the violaxanthin pool was exchanged for zeaxanthin. On the other hand, LHCII isolated from light-stressed leaves has been found to form lamellar aggregated structures in the plane of the lipid-protein membranes. Such structures are characterized by efficient excitation quenching in LHCII. The results of this study suggest that the physiological role of light-controlled antenna phosphorylation in the photosynthetic apparatus of plants, in addition to redistributing excitation energy and regulating the lateral reorganization of the thylakoid membrane, is to regulate the assembly of the thylakoid membranes into grana stacks by forming hydrogen bond–stabilized *trans*-layer skeletons. Another conclusion is that LHCII phosphorylation combined with violaxanthin deepoxidation facilitates protein assembly that protects the photosynthetic antenna network from overexcitation and photodegradation via nonradiative excitation energy dissipation.

METHODS

Chemicals

MGDG and DGDG lipids isolated from plants were purchased from Lipid Products Company. *n*-Dodecyl-β-ᴅ-maltoside (DM) and all the chemicals used in the lipid-LHCII membrane preparation were purchased from Sigma-Aldrich. All other chemical used in the preparations were of analytical grade.

Isolation of Nonphosphorylated and Partially Phosphorylated LHCII

LHCII was isolated from fresh spinach (*Spinacia oleracea*) leaves as described previously (Krupa et al., 1987), but to isolate phosphorylated LHCII, this method was slightly modified.

LHCII phosphorylation was achieved by illuminating fresh spinach leaves with high intensity light of 1200 μmol photons m^{-2} s^{-1} for 30 min. The photon flux density of 1200 μmol quanta m^{-2} s^{-1}, emitted by our light source, is equivalent to 1020 μmol photons m^{-2} s^{-1} of sunlight, in terms of the number of light quanta absorbed by thylakoids (see Supplemental Figure 1 online for the details of this calculation). Directly after illumination, leaves were ground in the buffer containing 20 mM Tricine, 0.4 M sorbitol, and 10 mM NaF, pH 7.8, and centrifuged for 5 min at 4°C and 5000g. The pellet was resuspended in 20 mM Tricine and 10 mM NaF buffer, pH 7.8, to a chlorophyll concentration of 0.8 mg mL^{-1}. Triton X-100 was added from a 5% stock solution to a final concentration of 0.7% (v/v). The suspension was incubated for 30 min at 21°C under continuous stirring. For precipitation of effective phosphorylated complexes, Triton X-100 was removed from the suspension by incubation overnight with Bio-beads adsorbent (Bio-Rad Laboratories). After removal of the detergent, the suspension was centrifuged for 40 min at 30,000g, and the supernatant was mixed with 1 M MgCl$_2$ and 1 M KCl to a final concentration of 100 mM KCl and 20 mM MgCl$_2$. The precipitated LHCII was purified by 40 min centrifugation at 15,000g on a Suc gradient. To obtain high purity of the preparation, the step involving protein precipitation with Triton X-100 and MgCl$_2$ and KCl was repeated and followed by a centrifugation for 40 min at 30,000g on a Suc gradient. Finally, pellet was washed two times in 20 mM Tricine buffer (centrifugation for 5 min at 40,000g) and was stored at −80°C. All the materials and buffers used were precooled.

The chlorophyll concentration was determined in 80% acetone according to Lichtenthaler (1987).

SDS-PAGE and Immunoblot Analysis

LHCII preparations were suspended in Laemmli denaturing buffer, and samples containing 1 μg of chlorophyll were loaded into polyacrylamide gel wells. After separation by standard SDS-PAGE electrophoresis, specific polypeptides were detected on the Polivinylidene difluoride membrane using primary antibodies against phospho-Thr (Cell Signaling) followed by anti-rabbit horseradish peroxidase conjugate and ECL detection system (Bio-Rad Laboratories). After detection of phosphor-Thr residues, the membrane was stripped by incubation in 62.5 mM Tris-HCl, pH 6.8, buffer containing 2% (w/v) SDS and 100 mM 2-mercaptoethanol and washing in 20 mM Tris-HCl, pH 7.5, buffer containing 0.5 M NaCl and 0.05% (v/v) Tween 20. Subsequently, the reaction with antibodies against Lhcb1 and Lhcb2 (Agrisera) with the same detection system was performed. Relative band intensities were quantified using the Quantity One software (Bio-Rad Laboratories).

Xanthophyll Analysis by HPLC

After isolation, LHCII samples were centrifuged at 11,000g for 5 min, and the pellet was dissolved in an acetonitrile:methanol:water (72:8:3, v:v:v) mixture. A C-18 filled, phase-reversed HPLC column (4.6 × 25 mm) was applied with a solvent system of acetonitrile:methanol:water (72:8:3, v:v:v) as a mobile phase. The flow rate was 0.8 mL/min. A Hewlett Packard HP 8453 spectrophotometer with absorption set at 441 nm was used as a detector. Absorption spectra of the separated fraction were recorded online between 280 and 900 nm in 10-s intervals. Xanthophyll pigments were identified on the basis of retention times and UV-Vis absorption spectra (see Supplemental Figure 4 online).

Preparation of Lipid-LHCII Membranes

MGDG and DGDG film (lipid molar ratio of 2:1, respectively) was deposited on glass test tubes via evaporation from the chloroform-methanol (2:1, v:v) solution under a stream of nitrogen. To remove traces of organic solvents, which may possibly remain in dry lipid films, the samples were placed in a vacuum (<10^{-5} bar) for 30 min. The LHCII complexes were suspended in 20 mM Tricine and 10 mM KCl buffer, pH 7.6, containing 0.03% DM. For incorporation of the LHCII complexes into lipid membranes, the LHCII samples were transferred to glass tubes and subjected to mild sonication in an ultrasonic bath for 30 min. The molar ratio of LHCII to lipids was 1:20. Next, DM was removed from the suspension by incubation with Bio-beads adsorbent at 4°C for 12 h. The lipid-LHCII membranes were separated from the detergent-free suspension by centrifugation at 15,000g for 5 min. Finally, the pellet was resuspended in 20 mM Tricine and 10 mM KCl buffer. A discussion regarding selection of a lipid-protein ratio is presented in Supplemental Methods 1 online (see also Supplemental References online).

The procedure applied yielded relatively small lipid-protein structures (nanodiscs), which assemble into larger topological forms during deposition to a solid support (see Supplemental Figure 6 online). Such a procedure has been elaborated to minimize the formation of large aggregated forms of LHCII characterized by the antiparallel orientation of the complexes, in which the N and C termini of neighboring trimers face the same direction. The thickness of the samples deposited to a solid support (~1.5 μm) was estimated by means of AFM measurements (see Supplemental Figure 9 online).

The lipid to protein molar ratio (20:1) was selected to reflect the very high protein crowding in the natural thylakoid membranes of plants. A detailed discussion related to the proportion of lipids and protein in the model system applied is presented in Supplemental Methods 1 online.

X-Ray Diffraction

Diffractometric measurements were performed using an Empyrean x-ray diffraction spectrometer from PANalytical with the CuK$_\alpha$ x-ray radiation λ = 0.154 nm. Before the experiments, the lipid and lipid-LHCII samples were deposited on the glass plate via evaporation from the buffer solution. The glass plate was washed with organic solvents. Diffractograms were collected from samples composed of approximately 250 lipid bilayers deposited on a 1-cm^2 area of glass plate. Data collection was in the 2Θ range of 0.6 to 26° with a step size of 0.01°.

77K Fluorescence Emission Spectroscopy

77K chlorophyll *a* fluorescence emission spectra were recorded from the lipid-LHCII samples using a Cary Eclipse spectrofluorometer (Varian) and the system described previously (Grudziński et al., 2001). The excitation wavelength was set at 470 nm. The excitation and emission slits were 10 and 5 nm, respectively.

FLIM

FLIM measurements were performed using a confocal LSM 780 system (Zeiss) coupled with an Observer Z.1 microscope. Samples were placed on nonfluorescent Menzel-Glaser #1 glass slides covered with poly-L-Lys. Fluorescence was excited at 440 nm by a LDH-PC-440B solid-state pulsed laser (PicoQuant) with a repetition rate of 20 MHz. Fluorescence photons were collected with the MPD detector. A 510-nm long-pass filter was placed on the detection path. Decay data analysis was performed using SymPhoTime (v. 5.0) software (PicoQuant).

Spectroscopy analysis was performed using the Grams/AI 8.0 software from ThermoGalactic. All the experiments were performed with

a minimum of five replicates, and the effects presented were found to be highly reproducible.

FTIR Absorption Spectroscopy

FTIR spectra were recorded with a Vector 33 spectrophotometer (Bruker). A clean crystal spectrum was used as a background. Liquid lipid-LHCII samples were deposited at CaF_2 transmission crystal by partial evaporation under a nitrogen stream. The spectra were recorded in the region between 4000 and 400 cm^{-1} at a resolution of one data point every 4 cm^{-1}. All the measurements were done in the dark and in a dry atmosphere at 21°C. Typically, 10 interferograms were collected, averaged, and Fourier transformed. Spectral analysis was performed with OPUS software (Bruker).

IR Absorption Imaging Microscopy

Lipid-LHCII and lipid-LHCII-HL samples, in the form of multibilayers, were deposited at the surface of an attenuated total internal reflection element in the form of a prism made of ZnSe monocrystals by the same method as in the preparation of samples for diffractometric analysis. The samples were scanned with the nano-IR microscopy system from Anasys Instruments. The IR imaging at the nanoresolution technique is based on AFM detection of an abrupt and temporary deformation of the scanned region of a sample. Such a deformation is caused by resonance absorption of IR radiation at a selected wave number, generated by the tunable and pulsed IR source (Policar et al., 2011; Marcott et al., 2012). Simultaneously, the system is able to scan a sample topography (with the conventional AFM technique), the image representing IR absorption (by the IR-AFM technique), and image representing the sample stiffness (related to the frequency of the AFM cantilever oscillations) (Policar et al., 2011; Marcott et al., 2012). The system also enables recording of the IR absorption spectra at the selected positions of the sample. All measurements were performed at room temperature.

Confocal Laser Scanning Microscopy and 3D Analysis

Lipid-LHCII samples were suspended in a 20 mM Tricine-NaOH buffer, pH 7.6, containing 10 mM KCl to chlorophyll concentration of 10 μg mL^{-1} and placed on ice and dark for 10 min. After incubation suspension was immobilized on a microscopy glass covered with poly-L-Lys (1 mg mL^{-1}). Samples were imaged using a Nikon A1 confocal laser scanning fluorescence microscope equipped with an Plan Apo TIRF ×100 oil differential interference contrast H (numerical aperture = 1.45) objective lens. An excitation beam was set at 561 nm from a diode laser working at minimal power to avoid photobleaching. Fluorescence emission was recorded in the range of 662 to 737 nm, while the confocal aperture was set at 1 Airy unit. Z-series (400 to 600 optical slices) of 512 × 512-pixel images taken from different focal planes were collected using a resonant scanner with a scan speed of 15 frames per second. Each optical slice was an average of 16 separate frames, and the distance in the Z-axis between two neighboring layers was set at 25 nm. To remove the spherical aberration effect and unspecific fluorescence signals, collected data stacks were subjected to a deconvolution procedure using the AutoQuant X3 software (Media Cybernetics). Deconvolved stacks, which had a 31 × 31 × 25-nm (X×Y×Z) voxel size, were used to create the three-dimensional models by Imaris 6.1.3 software (Bitplane).

Transmission Electron Microscopy

Electron microscopy was performed on a Leo 912AB transmission electron microscope (Zeiss) operated at 100 kV. Lipid-LHCII samples were deposited on a carbon-coated copper grid and negatively stained with 2% ammonium molybdate for 5 min. The calibrated magnification was ×31,000.

Molecular Modeling

The LHCII trimer model was visualized using VMD software support (http://www.ks.uiuc.edu/). VMD was developed, with support from the National Institutes of Health, by the Theoretical and Computational Biophysics group at the Beckman Institute, University of Illinois at Urbana-Champaign. LHCII coordinates were downloaded from the Protein Databank database (ID code: 2bhw).

Supplemental Data

The following materials are available in the online version of this article.

Supplemental Figure 1. Superimposed Spectra of the Sunlight, the Lamp Used to Preilluminate Leaves and One-Minus-Transmission Spectrum of the Thylakoid Suspension.

Supplemental Figure 2. SDS-PAGE and Immunoblot Control of the LHCII and LHCII-HL Preparation Purity.

Supplemental Figure 3. Immunoblot Analysis of the Phosphorylation Level of LHCII Isolated from Spinach Leaves.

Supplemental Figure 4. HPLC Chromatograms Showing Elution Peaks of the Xanthophyll Fraction of LHCII and LHCII-HL.

Supplemental Figure 5. Nano-IR and AFM Analyses of Lipid Multibilayers.

Supplemental Figure 6. Cryo-Electron Micrograph Showing the Lipid Membrane Fragments Modified with LHCII.

Supplemental Figure 7. CLSM Image of L-LHCII-HL Stained with DiOC$_{18}$(3) Membrane Lipid Dye.

Supplemental Figure 8. 77K Chlorophyll *a* Fluorescence Emission Spectra Recorded from LHCII and LHCII-HL in Trimeric and Aggregated Forms.

Supplemental Figure 9. AFM Image of the Lipid Multibilayer Deposited at the ZnSe Surface.

Supplemental Methods 1. Discussion on Selection of a LHCII-lipid Molar Ratio for Model Studies.

Supplemental References 1. References Cited in the Discussion on Selection of a LHCII-lipid Molar Ratio for Model Studies.

Supplemental Movie 1. Rotation of a structure L-LHCII.

Supplemental Movie 2. Rotation of a Structure L-LHCII-HL

Supplemental Movie Legend 1.

Supplemental Movie Legend 2.

REFERENCES

Ahn, T.K., Avenson, T.J., Ballottari, M., Cheng, Y.C., Niyogi, K.K., Bassi, R., and Fleming, G.R. (2008). Architecture of a charge-transfer state regulating light harvesting in a plant antenna protein. Science **320:** 794–797.

Allen, J.F. (1992). Protein phosphorylation in regulation of photosynthesis. Biochim. Biophys. Acta **1098:** 275–335.

Allen, J.F. (2003). Botany. State transitions—A question of balance. Science **299:** 1530–1532.

Austin, J.R., II., and Staehelin, L.A. (2011). Three-dimensional architecture of grana and stroma thylakoids of higher plants as determined by electron tomography. Plant Physiol. **155:** 1601–1611.

Barros, T., and Kuhlbrandt, W. (2009). Crystallisation, structure and function of plant light-harvesting complex II. Biochim. Biophys. Acta Bioenerg. **1787:** 753–772.

Barzda, V., Istokovics, A., Simidjiev, I., and Garab, G. (1996). Structural flexibility of chiral macroaggregates of light-harvesting chlorophyll a/b pigment-protein complexes. Light-induced reversible structural changes associated with energy dissipation. Biochemistry **35:** 8981–8985.

Belgio, E., Johnson, M.P., Jurić, S., and Ruban, A.V. (2012). Higher plant photosystem II light-harvesting antenna, not the reaction center, determines the excited-state lifetime-both the maximum and the nonphotochemically quenched. Biophys. J. **102:** 2761–2771.

Bennett, J. (1984). Thylakoid protein phosphorylation: *In vitro* and *in vivo.* Biochem. Soc. Trans. **12:** 771–774.

Bergantino, E., Dainese, P., Cerovic, Z., Sechi, S., and Bassi, R. (1995). A post-translational modification of the photosystem II subunit CP29 protects maize from cold stress. J. Biol. Chem. **270:** 8474–8481.

Chow, W.S., Kim, E.H., Horton, P., and Anderson, J.M. (2005). Granal stacking of thylakoid membranes in higher plant chloroplasts: The physicochemical forces at work and the functional consequences that ensue. Photochem. Photobiol. Sci. **4:** 1081–1090.

Chuartzman, S.G., Nevo, R., Shimoni, E., Charuvi, D., Kiss, V., Ohad, I., Brumfeld, V., and Reich, Z. (2008). Thylakoid membrane remodeling during state transitions in *Arabidopsis*. Plant Cell **20:** 1029–1039.

Cseh, Z., Rajagopal, S., Tsonev, T., Busheva, M., Papp, E., and Garab, G. (2000). Thermooptic effect in chloroplast thylakoid membranes. Thermal and light stability of pigment arrays with different levels of structural complexity. Biochemistry **39:** 15250–15257.

Cseh, Z., Vianelli, A., Rajagopal, S., Krumova, S., Kovács, L., Papp, E., Barzda, V., Jennings, R., and Garab, G. (2005). Thermo-optically induced reorganizations in the main light harvesting antenna of plants. I. Non-Arrhenius type of temperature dependence and linear light-intensity dependencies. Photosynth. Res. **86:** 263–273.

Depège, N., Bellafiore, S., and Rochaix, J.D. (2003). Role of chloroplast protein kinase Stt7 in LHCII phosphorylation and state transition in Chlamydomonas. Science **299:** 1572–1575.

Dobrikova, A.G., Várkonyi, Z., Krumova, S.B., Kovács, L., Kostov, G.K., Todinova, S.J., Busheva, M.C., Taneva, S.G., and Garab, G. (2003). Structural rearrangements in chloroplast thylakoid membranes revealed by differential scanning calorimetry and circular dichroism spectroscopy. Thermo-optic effect. Biochemistry **42:** 11272–11280.

Douce, R., and Joyard, J. (1996). Biosynthesis of thylakoid membrane lipids. In Oxygenic Photosynthesis: The Light Reactions, D.R. Ort and C.F. Yocum, eds (Dordrecht, The Netherlands: Springer), pp. 69–101.

Frank, H.A., Bautista, J.A., Josue, J.S., and Young, A.J. (2000). Mechanism of nonphotochemical quenching in green plants: Energies of the lowest excited singlet states of violaxanthin and zeaxanthin. Biochemistry **39:** 2831–2837.

Fristedt, R., Willig, A., Granath, P., Crèvecoeur, M., Rochaix, J.D., and Vener, A.V. (2009). Phosphorylation of photosystem II controls functional macroscopic folding of photosynthetic membranes in *Arabidopsis*. Plant Cell **21:** 3950–3964.

Garab, G., Lohner, K., Laggner, P., and Farkas, T. (2000). Self-regulation of the lipid content of membranes by non-bilayer lipids: A hypothesis. Trends Plant Sci. **5:** 489–494.

Garab, G., and Mustardy, L. (1999). Role of LHCII-containing macrodomains in the structure, function and dynamics of grana. Aust. J. Plant Physiol. **26:** 649–658.

Garstka, M., Drozak, A., Rosiak, M., Venema, J.H., Kierdaszuk, B., Simeonova, E., van Hasselt, P.R., Dobrucki, J., and Mostowska, A. (2005). Light-dependent reversal of dark-chilling induced changes in chloroplast structure and arrangement of chlorophyll-protein complexes in bean thylakoid membranes. Biochim. Biophys. Acta **1710:** 13–23.

Garstka, M., Venema, J.H., Rumak, I., Gieczewska, K., Rosiak, M., Koziol-Lipinska, J., Kierdaszuk, B., Vredenberg, W.J., and Mostowska, A. (2007). Contrasting effect of dark-chilling on chloroplast structure and arrangement of chlorophyll-protein complexes in pea and tomato: plants with a different susceptibility to non-freezing temperature. Planta **226:** 1165–1181.

Goral, T.K., Johnson, M.P., Brain, A.P.R., Kirchhoff, H., Ruban, A.V., and Mullineaux, C.W. (2010). Visualizing the mobility and distribution of chlorophyll proteins in higher plant thylakoid membranes: Effects of photoinhibition and protein phosphorylation. Plant J. **62:** 948–959.

Goral, T.K., Johnson, M.P., Duffy, C.D.P., Brain, A.P.R., Ruban, A.V., and Mullineaux, C.W. (2012). Light-harvesting antenna composition controls the macrostructure and dynamics of thylakoid membranes in *Arabidopsis*. Plant J. **69:** 289–301.

Grudziński, W., Matuła, M., Sielewiesiuk, J., Kernen, P., Krupa, Z., and Gruszecki, W.I. (2001). Effect of 13-cis violaxanthin on organization of light harvesting complex II in monomolecular layers. Biochim. Biophys. Acta **1503:** 291–302.

Gruszecki, W.I., Gospodarek, M., Grudziński, W., Mazur, R., Gieczewska, K., and Garstka, M. (2009a). Light-induced change of configuration of the LHCII-bound xanthophyll (tentatively assigned to violaxanthin): A resonance Raman study. J. Phys. Chem. B **113:** 2506–2512.

Gruszecki, W.I., Grudzinski, W., Gospodarek, M., Patyra, M., and Maksymiec, W. (2006). Xanthophyll-induced aggregation of LHCII as a switch between light-harvesting and energy dissipation systems. Biochim. Biophys. Acta **1757:** 1504–1511.

Gruszecki, W.I., Janik, E., Luchowski, R., Kernen, P., Grudzinski, W., Gryczynski, I., and Gryczynski, Z. (2009b). Supramolecular

organization of the main photosynthetic antenna complex LHCII: A monomolecular layer study. Langmuir **25:** 9384–9391.

Gruszecki, W.I., and Sielewiesiuk, J. (1991). Galactolipid multibilayers modified with xanthophylls: Orientational and diffractometric studies. Biochim. Biophys. Acta **1069:** 21–26.

Gruszecki, W.I., Zubik, M., Luchowski, R., Janik, E., Grudzinski, W., Gospodarek, M., Goc, J., Fiedor, L., Gryczynski, Z., and Gryczynski, I. (2010). Photoprotective role of the xanthophyll cycle studied by means of modeling of xanthophyll–LHCII interactions. Chem. Phys. **373:** 122–128.

Hasegawa, M., Shiina, T., Terazima, M., and Kumazaki, S. (2010). Selective excitation of photosystems in chloroplasts inside plant leaves observed by near-infrared laser-based fluorescence spectral microscopy. Plant Cell Physiol. **51:** 225–238.

Hohmann-Marriott, M.F., and Blankenship, R.E. (2011). Evolution of photosynthesis. Annu. Rev. Plant Biol. **62:** 515–548.

Holm, J.K., Várkonyi, Z., Kovács, L., Posselt, D., and Garab, G. (2005). Thermo-optically induced reorganizations in the main light harvesting antenna of plants. II. Indications for the role of LHCII-only macrodomains in thylakoids. Photosynth. Res. **86:** 275–282.

Horton, P. (2012). Optimization of light harvesting and photoprotection: Molecular mechanisms and physiological consequences. Philos. Trans. R. Soc. Lond. B Biol. Sci. **367:** 3455–3465.

Iwai, M., Takahashi, Y., and Minagawa, J. (2008). Molecular remodeling of photosystem II during state transitions in *Chlamydomonas reinhardtii*. Plant Cell **20:** 2177–2189.

Iwai, M., Yokono, M., Inada, N., and Minagawa, J. (2010). Live-cell imaging of photosystem II antenna dissociation during state transitions. Proc. Natl. Acad. Sci. USA **107:** 2337–2342.

Jahns, P., Wehner, A., Paulsen, H., and Hobe, S. (2001). De-epoxidation of violaxanthin after reconstitution into different carotenoid binding sites of light-harvesting complex II. J. Biol. Chem. **276:** 22154–22159.

Johnson, M.P., Goral, T.K., Duffy, C.D.P., Brain, A.P.R., Mullineaux, C.W., and Ruban, A.V. (2011). Photoprotective energy dissipation involves the reorganization of photosystem II light-harvesting complexes in the grana membranes of spinach chloroplasts. Plant Cell **23:** 1468–1479.

Kirchhoff, H. (2008a). Molecular crowding and order in photosynthetic membranes. Trends Plant Sci. **13:** 201–207.

Kirchhoff, H. (2008b). Significance of protein crowding, order and mobility for photosynthetic membrane functions. Biochem. Soc. Trans. **36:** 967–970.

Kirchhoff, H., Haferkamp, S., Allen, J.F., Epstein, D.B.A., and Mullineaux, C.W. (2008b). Protein diffusion and macromolecular crowding in thylakoid membranes. Plant Physiol. **146:** 1571–1578.

Kirchhoff, H., Lenhert, S., Büchel, C., Chi, L., and Nield, J. (2008a). Probing the organization of photosystem II in photosynthetic membranes by atomic force microscopy. Biochemistry **47:** 431–440.

Kouřil, R., Dekker, J.P., and Boekema, E.J. (2012). Supramolecular organization of photosystem II in green plants. Biochim. Biophys. Acta **1817:** 2–12.

Kouril, R., Oostergetel, G.T., and Boekema, E.J. (2011). Fine structure of granal thylakoid membrane organization using cryo electron tomography. Biochim. Biophys. Acta Bioenerg. **1807:** 368–374.

Krupa, Z., Huner, N.P., Williams, J.P., Maissan, E., and James, D.R. (1987). Development at cold-hardening temperatures. The structure and composition of purified rye light harvesting complex II. Plant Physiol. **84:** 19–24.

Lahiri, B., Holland, G., and Centrone, A. (2013). Chemical imaging beyond the diffraction limit: Experimental validation of the PTIR technique. Small **9:** 439–445.

Lichtenthaler, H.K. (1987). Chlorophylls and carotenoids: Pigments of photosynthetic biomembranes. Methods in Enzymology, **148:** 350–382.

Marcott, C., Kjoller, K., Lo, M., Prater, C., Shetty, R., and Dazzi, A. (2012). Nanoscale IR spectroscopy: AFM-IR - a new technique. Spectroscopy **27:** 60–65.

Mehta, M., Sarafis, V., and Critchley, C. (1999). Thylakoid membrane architecture. Aust. J. Plant Physiol. **26:** 709–716.

Mustárdy, L., Buttle, K., Steinbach, G., and Garab, G. (2008). The three-dimensional network of the thylakoid membranes in plants: Quasihelical model of the granum-stroma assembly. Plant Cell **20:** 2552–2557.

Mustárdy, L., and Garab, G. (2003). Granum revisited. A three-dimensional model—where things fall into place. Trends Plant Sci. **8:** 117–122.

Policar, C., Waern, J.B., Plamont, M.A., Clède, S., Mayet, C., Prazeres, R., Ortega, J.M., Vessières, A., and Dazzi, A. (2011). Subcellular IR imaging of a metal-carbonyl moiety using photothermally induced resonance. Angew. Chem. Int. Ed. Engl. **50:** 860–864.

Rintamäki, E., Salonen, M., Suoranta, U.M., Carlberg, I., Andersson, B., and Aro, E.M. (1997). Phosphorylation of light-harvesting complex II and photosystem II core proteins shows different irradiance-dependent regulation in vivo. Application of phosphothreonine antibodies to analysis of thylakoid phosphoproteins. J. Biol. Chem. **272:** 30476–30482.

Ruban, A.V., Dekker, J.P., Horton, P., and van Grondelle, R. (1995). Temperature-dependence of chlorophyll fluorescence from the light-harvesting complex II of higher plants. Photochem. Photobiol. **61:** 216–221.

Ruban, A.V., Johnson, M.P., and Duffy, C.D.P. (2012). The photoprotective molecular switch in the photosystem II antenna. Biochim. Biophys. Acta Bioenerg. **1817:** 167–181.

Ruban, A.V., Phillip, D., Young, A.J., and Horton, P. (1997). Carotenoid-dependent oligomerization of the major chlorophyll a/b light harvesting complex of photosystem II of plants. Biochemistry **36:** 7855–7859.

Rumak, I., Gieczewska, K., Kierdaszuk, B., Gruszecki, W.I., Mostowska, A., Mazur, R., and Garstka, M. (2010). 3-D modelling of chloroplast structure under (Mg^{2+}) magnesium ion treatment. Relationship between thylakoid membrane arrangement and stacking. Biochim. Biophys. Acta **1797:** 1736–1748.

Rumak, I., Mazur, R., Gieczewska, K., Kozioł-Lipińska, J., Kierdaszuk, B., Michalski, W.P., Shiell, B.J., Venema, J.H., Vredenberg, W.J., Mostowska, A., and Garstka, M. (2012). Correlation between spatial (3D) structure of pea and bean thylakoid membranes and arrangement of chlorophyll-protein complexes. BMC Plant Biol. **12:** 72.

Shimoni, E., Rav-Hon, O., Ohad, I., Brumfeld, V., and Reich, Z. (2005). Three-dimensional organization of higher-plant chloroplast thylakoid membranes revealed by electron tomography. Plant Cell **17:** 2580–2586.

Simidjiev, I., Stoylova, S., Amenitsch, H., Javorfi, T., Mustardy, L., Laggner, P., Holzenburg, A., and Garab, G. (2000). Self-assembly of large, ordered lamellae from non-bilayer lipids and integral membrane proteins in vitro. Proc. Natl. Acad. Sci. USA **97:** 1473–1476.

Tamm, L.K., and Tatulian, S.A. (1997). Infrared spectroscopy of proteins and peptides in lipid bilayers. Q. Rev. Biophys. **30:** 365–429.

Tikkanen, M., and Aro, E.M. (2012). Thylakoid protein phosphorylation in dynamic regulation of photosystem II in higher plants. Biochim. Biophys. Acta **1817:** 232–238.

Tikkanen, M., Grieco, M., and Aro, E.M. (2011). Novel insights into plant light-harvesting complex II phosphorylation and 'state transitions'. Trends Plant Sci. **16:** 126–131.

van Oort, B., van Hoek, A., Ruban, A.V., and van Amerongen, H. (2007). Aggregation of light-harvesting complex II leads to formation of efficient excitation energy traps in monomeric and trimeric complexes. FEBS Lett. **581:** 3528–3532.

Wada, H., and Murata, N. (2010). Lipids in Photosynthesis: Essential and Regulatory Functions. (New York: Springer).

Zer, H., Vink, M., Keren, N., Dilly-Hartwig, H.G., Paulsen, H., Herrmann, R.G., Andersson, B., and Ohad, I. (1999). Regulation of thylakoid protein phosphorylation at the substrate level: Reversible light-induced conformational changes expose the phosphorylation site of the light-harvesting complex II. Proc. Natl. Acad. Sci. USA **96:** 8277–8282.

Zubik, M., Luchowski, R., Puzio, M., Janik, E., Bednarska, J., Grudziński, W., and Gruszecki, W.I. (2013). The negative feedback molecular mechanism which regulates excitation level in the plant photosynthetic complex LHCII: Towards identification of the energy dissipative state. Biochim. Biophys. Acta **1827:** 355–364.